Different Bandgaps in $Cu_2ZnSnSe_4$: A High Temperature Coevaporation Study

Alex Redinger, Jan Sendler, Rabie Djemour, Thomas P. Weiss, Germain Rey, Phillip J. Dale, and Susanne Siebentritt

***Abstract*—We present a high-temperature $Cu_2ZnSnSe_4$ coevaporation study, where solar cells with a power conversion efficiency of 7.1% have been achieved. The process is monitored with laser light scattering in order to follow the incorporation of the Sn into the film. We observe the segregation of ZnSe at the Mo/CZTSe interface. Optical analysis has been carried out with photoluminescence and spectrophotometry. We observe strong band tailing and a bandgap, which is significantly lower than in other reported efficient CZTSe absorbers. The photoluminescence at room temperature is lower than the bandgap due to the existence of a large quantity of tail states. Finally, we present effects of low-temperature postannealing of the absorbers on ordering of the Cu/Zn atoms in CZTSe and solar cell parameters. We observe strong changes in all solar cell parameters upon annealing. The efficiency of the annealed devices is significantly reduced, although ordering is improved compared with ones made from nonannealed absorbers.**

***Index Terms*—$Cu_2ZnSnSe_4$, coevaporation, order–disorder, solar cells.**

I. Introduction

$Cu_2ZnSnSe_4$ thin-film solar cells are extensively studied as absorber layers for thin-film solar cells. Although substantial progress has been made in recent years, record efficiencies are still far away from other thin-film technologies such as $Cu(In,Ga)Se_2$ and CdTe [1]. The reasons for the lower efficiencies are manifold. The most prominent ones are low minority carrier lifetimes [2] and secondary phases [3]. In addition, CZTSe solar cells usually exhibit a weak low-energy response in the quantum efficiency (QE) measurements, which is attributed to a large number of tail states [4].

In this paper, we would like to study this effect of band tailing/bandgap fluctuations in more detail. The study is limited to pure selenide absorbers, where S/Se variations are ruled out. Currently, the best performing selenide devices are produced at IMEC and a 10.4% solar cell has been reported [5]. The best performing coevaporated samples are currently produced at NREL, and the current record device is 9.15% [6]. The bandgap of CZTSe, as reported by Brammertz *et al.*, is roughly 1.0 eV [7]; it has been deduced from the QE and from room temperature photoluminescence (RT-PL) measurements. Repins *et al.* [6] reported a slightly lower bandgap of 0.96 eV as deduced from RT-PL. In another study, Shin *et al.* [8] have reported a 8.9% CZTSe solar cell. They observed that depending on the Se partial pressure during the final heat treatment, different room temperature PL transitions are observed. At the highest partial pressure, the main transition can be found at roughly 1 eV. Lowering the partial pressure leads to PL transitions at lower energies. They proposed that the PL transitions originate from the formation of deep defects if the Se partial pressure is not high enough. In our recent studies on CZTSe solar cells produced via coevaporation and annealing [3], [9], we proposed a different explanation for the observed PL transitions, which are in fact due to various band-to-band transitions. There is a substantial variation of the apparent bandgaps deduced from QE. We measured variations between 0.96 and 0.90 eV, which is consistent with the RT-PL data. From intensity-dependent measurements of the PL peaks, it follows that these transitions are band to band [9].

Here, we use high-temperature coevaporation to produce efficient CZTSe absorbers, and we analyze the absorbers by PL, spectrophotometry, and QE. Moreover, low-temperature postannealings of absorbers have been carried out in order to change the Cu/Zn ordering in the CZTSe absorbers. A second-order phase transition has been observed in CZTS [10] and CZTSe [11], and we have recently shown that the amount of ordering is also changing the bandgap of CZTSe [11].

II. Experimental Details

The CZTSe absorbers have been grown via high-temperature coevaporation in a molecular beam epitaxy system. The metals (Zn, Sn, Cu) are evaporated from effusion cells, and the selenium is supplied via a valved cracker source. The cracker is heated to 1000 °C during growth in order to enhance the reactivity of the selenium. In order to prevent the high-temperature decomposition of CZTSe [12], we use an additional SnSe effusion cell to further increase the SnSe supersaturation. A maximum substrate temperature of 470 °C during growth has been chosen. The temperature is measured with a pyrometer. Compared with the current record coevaporated CZTSe devices, we are able to use a much lower selenium overpressure (roughly a factor of eight less compared to the value given in [13]). Device finishing includes a 30-s 5 wt% KCN etching step, a chemical bath-deposited CdS layer followed by an undoped and Al-doped ZnO window layer, and a Ni–Al grid. We also compared our coevaporated devices with samples produced by a sequential route as described

Manuscript received July 7, 2014; revised November 13, 2014; accepted November 21, 2014. Date of publication December 24, 2014; date of current version February 18, 2015. This work was supported by the Luxembourgish Fonds National de la Recherche in the framework of the KITS2 Project. The work of J. Sendler was supported by the European initial training network program Kestcells through Project FP7-PEOPLE-2012-ITN 316488.

A. Redinger, J. Sendler, R. Djemour, T. P. Weiss, G. Rey, and S. Siebentritt are with the Laboratory for Photovoltaics and the Physics and Material Research Unit, University of Luxembourg, L-4367 Belvaux, Luxembourg (e-mail: redingeralex@gmail.com; jan.sendler@uni.lu; rabie.djemour@uni.lu; thomas.weiss@uni.lu; germain.rey@uni.lu; susanne.siebentritt@uni.lu).

P. J. Dale is with the Laboratory for Energy Materials and the Physics and Material Research Unit, University of Luxembourg, L-4367 Belvaux, Luxembourg (e-mail: phillip.dale@uni.lu).

Color versions of one or more of the figures in this paper are available online at http://ieeexplore.ieee.org.

Digital Object Identifier 10.1109/JPHOTOV.2014.2377561

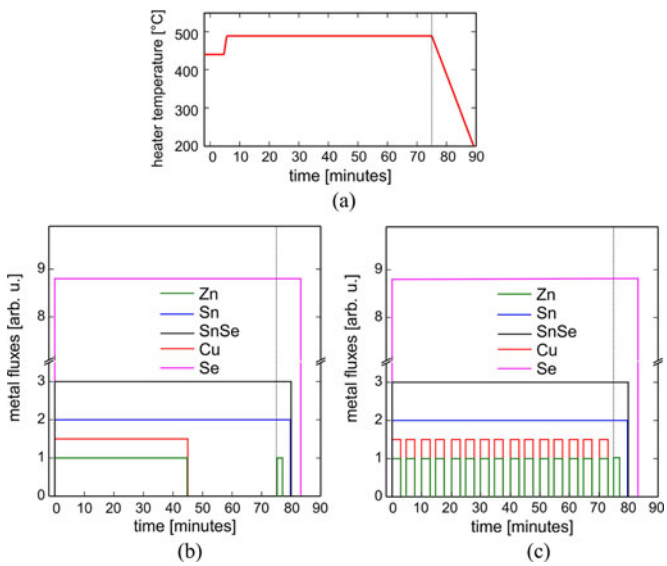

Fig. 1. (a) Temperature profile of the substrate heater during growth. (b) and (c) Element fluxes during growth (for details, see the text). The vertical dotted line depicts the start of the cooling down.

in [3], where the coevaporation has been performed at roughly 320 °C followed by a postannealing at 500 °C in a tube furnace.

The solar cells have been characterized with a home-built current–voltage setup equipped with a cold mirror halogen lamp adjusted to an intensity of 1000 W/m^2. In addition, we performed QE measurements, temperature-dependent current–voltage analysis to study the dominant recombination pathway, and the evolution of the series resistance and capacitance–voltage measurements to extract the doping density. We measure $C(V)$ at room temperature and deduce the doping density from Mott–Schottky plots. We use the part of the curve under small forward bias to do the fitting and to extract the built-in potential and the doping density. The absorber composition has been measured with an energy dispersive X-Ray analysis system (EDX). We performed room temperature PL with 514.5-nm excitation and absorption measurements with a UV/VIS/NIR spectrophotometer to determine the bandgap of the grown samples. The transmittance and reflectance of the films have been measured from absorbers grown on glass substrates during the same process as the ones on molybdenum-coated glass substrates used for solar cells. The thickness of the absorber layers is measured via SEM cross-sectional images. Transmission, reflection, and film thickness are sufficient to calculate the absorption coefficient from which the bandgap and the Urbach tails can be deduced (see, for example, [14]).

III. Absorber Growth

The growth processes and the heater temperature used in this study are schematically depicted in Fig. 1. The growth is started at 440 °C heater temperature [see Fig. 1(a)]. After 5 min, the heater temperature is raised to 490 °C and is kept constant for the rest of the growth processes. In the following, this low-temperature step at the beginning of the process is denoted as onset temperature. The idea behind the lower onset temperature was to promote the sticking of Sn and SnSe at the beginning of the process and to completely prevent the formation of large amounts of ZnSe as described already in earlier experiments [15]. However, as we will see in the following, this reduction of the temperature was not sufficient to prevent the formation of ZnSe at the back of the absorber. Finally, the temperature is decreased, and the samples are cooled down naturally to 200 °C. The time of the cooling down from 490 °C to 200 °C heater temperature takes 14 min. At 200 °C, the sample is removed from the reactor into the load-lock, which is vented to take the sample out of the chamber. The sample can be considered as quenched from 200 °C to room temperature. These details of the final cool down to room temperature are usually not given in the literature, since it is assumed that all relevant processes happen at the growth temperature or during the initial period of the cool down. It turns out that this last cool down to room temperature is important for CZTSe.

Fig. 1(b) and (c) shows how the element fluxes are regulated during the processes. The process in Fig. 1(b) is very similar to the growth process introduced by NREL [6] and is divided into two main stages. In the first step, all five shutters of the sources are open, and Cu, Zn, Sn, SnSe and Se are coevaporated for 45 min followed by a second step, where the Cu and Zn fluxes are switched OFF. After 90 min, the process ends. During cool down, Zn is supplied for an additional 2 min in order to produce a Zn-rich surface termination, which has been reported to be beneficial for device performance [2]. After 5 min of cool down, the Sn and SnSe are switched OFF. This is necessary to prevent decomposition of CZTSe. At 300 °C pyrometer temperature, the Se flux is switched OFF. The two-stage process is necessary, since the reaction of all constituents is slow. It has been shown by Kaune *et al.* [16] that after the first stage, there is a substantial amount of Cu_xSe present in the CZTSe absorbers. Only during the second stage, where no Cu is supplied, the system has enough time to fully react and the Cu_xSe are consumed, which is prerequisite for working devices. Some of the samples presented here are also grown by a different process depicted in Fig. 1(c). Here, the two-stage process presented in Fig. 1(b) is divided into many small steps. In analogy to the former process, a stage where all elements are coevaporated and a stage without Cu and Zn evaporation are iterated. This eliminates the need for an additional long annealing stage since the Cu_xSe are reacted away earlier.

The evolution of the growth is monitored with laser light scattering (635-nm laser diode chopped at 2 kHz) and with a pyrometer (range of measurement between 2 and 2.6 μm). The results are presented in Fig. 2. The process depicted in Fig. 2 is roughly 30 min longer than depicted in Fig. 1(b) and (c) in order to account for differences in the metal fluxes. Moreover, the film thickness is slightly larger than the film depicted in Fig. 1. The process is not a copy of the process in Fig. 1, but these samples have been grown in order to study the time evolution of the composition during the process. The results discussed for this longer process are also valid for the shorter process depicted in Fig. 1(c). Immediately after the start of the growth, the laser light scattering signal (LLS) signal drops sharply. Heating the

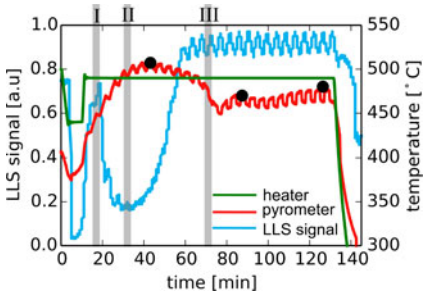

Fig. 2. Heater temperature, pyrometer temperature, and LLS as a function of process time for a growth sequence depicted in Fig. 1(c). The vertical lines labeled (I, II, III) depict the positions, where break-off experiments have been performed. The black dots depict the maxima of the thickness interference fringes.

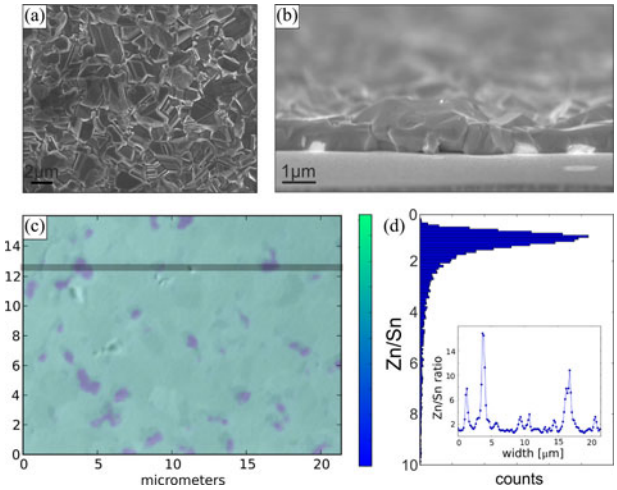

Fig. 3. (a) SEM topview of a CZTSe absorber grown with the process depicted in Fig. 1(c). (b) Cross section of the same absorber; the sample has been tilted by 5 °C toward the camera. (c) EDX mapping of the backsurface of the same absorber. (d) Computed histogram of the Zn/Sn ratio.

substrate to 490 °C after 5 min leads to a strong increase in the LLS signal. In order to study the composition during the different stages of growth, break-off experiments have been performed, which are labeled (I, II, III) in Fig. 2. At the position (I), the amount of Sn in the film is roughly 1 at%, which is probably caused by the cool down procedure. The cool down procedure has been developed to prevent decomposition of CZTSe. However, in this case, the film does not consist of CZTSe but mainly of $Cu_{2-x}Se$ and ZnSe. Consequently, there is a chance that during cool down, some of the $Cu_{2-x}Se$ reacts to Cu_2SnSe_3 or CZTSe, since Sn and SnSe are supplied for the first 5 min of the cool down. An alternative explanation is that the amount of Sn in the first stage is independent of the cool down, but there is only a small amount of CZTSe present during that time.

The height of the LLS peak labeled (I) can be altered by the onset temperature during the initial period of growth. At 300 °C and below, the peak vanishes. The LLS signal levels out after roughly 30 min. A break-off experiment at the position labeled (II) shows that the Sn in the film is increasing but remains rather low (at roughly 3 at%). After about 45 min, the LLS signal increases and levels out again after 70 min. EDX analysis of the break-off experiment shows that Sn is now incorporating into the film. The Sn content is at roughly 10 at% and the Zn content at 12 at%. For the rest of the growth, the LLS signal stays flat, except the small changes induced by the opening and closing of the shutters as depicted in Fig. 1(c). The measured composition of the film is still changing a bit presumably due to changes in the interaction volume of the EDX measurement as a consequence of the different film thickness between (III) and the final film. After the end of the process, the sample is slightly Sn-rich (Zn/Sn = 0.94) and Cu-poor (Cu/(Zn + Sn) = 0.90). The solar cell efficiency of this process reached 5.9%. Solar cells made from the break-off experiment did not give working devices. The results are in according with earlier results [15], [16]. The pyrometer signal shown in Fig. 2 shows damped and highly distorted thickness interference fringes. The maxima are labeled with a black dots in Fig. 2. The oscillation frequency is longer during the first hour, and then, the frequency, although strongly damped, increases. This is in line with the preceding discussion and results discussed in [17]. During the first 60 min, the Sn incorporation is low and incomplete. Consequently, the speed of growth is lower than in the second half of the process. The low-amplitude changes with a period of a few minutes in both signals of Fig. 2 are due to opening and closing of the shutter. The preceding discussion shows that the incorporation of Sn into the film can be monitored by the LLS signal and by changes in the oscillation frequency of the pyrometer signal. The peak at position (I) in Fig. 2 is currently attributed to the onset of Sn incorporation. However, it has to be emphasized that the peak can also be correlated with the ramping up of the substrate to growth temperature. Therefore, other effects such as changes in roughness cannot be excluded. In any case, the measurement provides a powerful way to monitor the composition of the film during growth.

IV. Characterization

Fig. 3 depicts exemplary SEM and EDX analysis of an absorber grown with the process depicted in Fig. 1(c). The following results are, however, also valid for the process depicted in Fig. 1(b). In Fig. 3(a), a top-view micrograph is shown. The sample consists of large compact grains with extensions of several micrometers. Fig. 3(b) shows a cross section of the same absorber. The sample has been tilted by 5° toward the secondary electron detector in order to improve the visibility at the CZTSe/Mo interface. Large white patches are visible at the interface. In order to further analyze this secondary phase, the absorber has been mechanically removed with the help of glue, and the backsurface of the film has been analyzed with energy dispersive X-Ray analysis mapping. The result is shown in Fig. 3(c), where the deduced Zn/Sn ratio (calculated via full EDX spectrum fitting) is color coded and overlaid on the SEM micrograph. The Zn/Sn ratio varies strongly as a function of position and the extension of the high-Zn-content regions are on the order of 1 μm. Fig. 3(d) shows a histogram and a linescan of the Zn/Sn ratios that are shown in Fig. 3(c). It is clearly visible that the Zn/Sn is close to unity in the majority of the

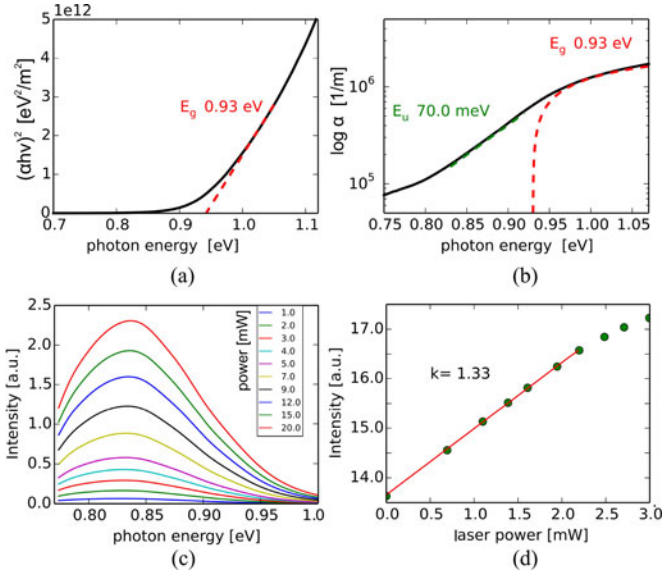

Fig. 4. (a) $(\alpha h\nu)^2$ plot to extract the bandgap. (b) Logarithm of the absorption coefficient as a function of photon energy to extract the bandgap and the Urbach energy. (c) RT-PL measurements at different laser intensities. (d) Log–log plot of the laser intensity as a function of the PL yield to extract the k-value.

backsurface, except in the regions where the Zn rich patches are present. Based on the preceding analysis and other literature reports [15], [16], [18], we conclude that there is a large amount of ZnSe still present at the Mo/CZTSe interface despite the somewhat lower onset temperature during growth and the high Sn and Se overpressures during growth. Since Sn is not incorporated in the beginning of the growth process, ZnSe and $Cu_x Se$ are formed. The $Cu_x Se$ is consumed in the process of the growth, but the ZnSe patches remain and stay at the Mo/CZTSe interface. A further reduction of the onset temperature from 440 °C to 300 °C drastically reduces the amount of ZnSe at the back (data not shown). However, we have yet to observe an improvement of the solar cell efficiency.

The measured optical properties of the absorbers are depicted in Fig. 4. The absorption coefficient has been extracted from transmittance and reflectance measurements of samples grown on glass substrates. It has to be emphasized that this absorption coefficient is very similar to the one measured from absorbers, which have been mechanically removed from the Mo-coated glass substrates. The advantage is that the samples are larger, and consequently, the measurement procedure is simpler. The absorption coefficient α has been calculated from transmittance and reflectance as described in [11]. The result is shown in Fig. 4(a), where the $(\alpha h\nu)^2$ plot is presented and in Fig. 4(b) where the logarithm of the absorption coefficient as a function of the photon energy is shown. From Fig. 4(a), the extraction of the bandgap is difficult. The transition is not abrupt but gradual, and consequently, the identification of the bandgap E_g is ambiguous. Therefore, the absorption coefficient has been plotted on a logarithmic scale in order to identify the transition from the square root dependence of the direct bandgap to the exponential dependence of the Urbach tail states [19]. From Fig. 4(b), it is easy to find the region of the tail states, i.e., the linear regime in the log plot. A value of 70 meV can be extracted from the plot, which is extremely large. The direct bandgap has to be located at higher energies. An approximate value of 0.93 eV can be extracted as shown in Fig. 4(b) and also indicated in Fig. 4(a).

A large Urbach energy indicates that there are a lot of states in the bandgap in proximity to the band edge energies, which are likely to be localized. The value of 70 meV is comparable with Urbach energies measured in amorphous silicon [20]. This material class is completely disordered, which gives rise to large exponential tails at the bandgap edges. We, therefore, have to assume that disorder is also present in our coevaporated CZTSe samples. In fact, an order–disorder transition from the kesterite structure ($I\bar{4}$) to the disordered kesterite structure ($I\bar{4}2$ m) has recently been found in sulfur-based absorbers [10]. In the ordered $I\bar{4}$ material, all Cu and Zn atoms in the unit cell are at well-defined Wyckoff positions. If the substrate temperature is high enough, some of the zinc at the wyckoff position 2c in the ordered kesterite is occupied by Cu, and some of the 2d Cu sites are occupied with zinc [21]. Schorr [21] already pointed out that the ordering crucially depends on the cooling rate. Slow cooling leads to more ordered material, whereas quenching leads to disordered material. The transition temperature of the second-order phase transition in CZTS is 260 °C as measured in [10]. Recently, we could show that selenium based CZTSe exhibit the same transition at slightly lower temperatures 200 ± 10 °C [11]. In particular, we could show that the bandgap, which is deduced from absorption measurements, changes with different degrees of ordering. We attribute at least part of the disorder responsible for the Urbach tailing to the simultaneous presence of ordered and disordered kesterite.

Some further consequences of ordering and disordering will be discussed in the next paragraphs. First, we would like to present another important outcome of the optical characterization. Fig. 4(c) depicts RT-PL measurements, which, in contrast with our absorbers grown by a sequential process, only show one single PL peak. The sample has been measured at different laser excitations in order to identify the nature of the measured transition. The measured PL transition is at 0.83 eV, which is significantly lower than bandgap energy deduced from absorption measurements. The peak does not shift with increasing power excitation. The PL yield as a function of the laser power excitation is shown in Fig. 4(d) on a log–log scale. The slope k of the curve is equal to the exponent of the power law. We deduce a k-value of 1.33. We have measured the same behavior on several samples and at several positions on those samples. A k-value between 1 and 2 and the absence of a change of the peak position with laser excitation is a clear indication that the transition is band to band [22]. Comparing the results from the absorption measurements with the PL results, we have to conclude that the bandgap energy is not the same. There is a discrepancy of almost 100 meV between the PL measurement shown in Fig. 4(c) and the bandgap presented in Fig. 4(a). The same observation has been made by Gokmen *et al.* [4] in CZTSSe. They showed, in agreement with the above analysis, that there is a substantial amount of band tailing in the CZTSSe. They attributed the redshift in PL to electrostatic potential fluctuations and/or

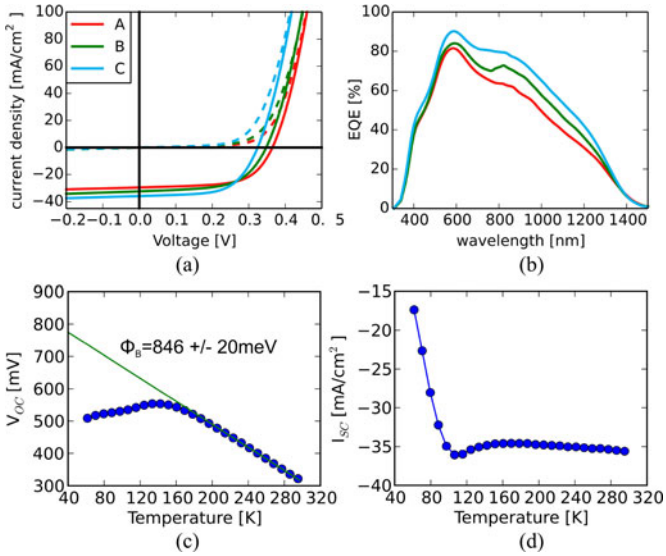

Fig. 5. (a) Current–voltage characteristics of three efficient devices and (b) their corresponding QE, (c) temperature dependence of the open-circuit voltage, and (d) temperature dependence of the short-circuit current density.

bandgap fluctuations. Moreover, recent results point toward a strong disorder in the CZTSe system, which may lead to effects that are usually not observed in crystalline well-ordered materials. The generated electron–hole pairs can thermalize into the region of the band tails. Since the number of localized states is large, there is a quite high chance that the carriers can thermalize quite far into the tail states before they recombine. A k-value larger than 1 can be expected since the number of available localized states is large, and therefore, the probability of radiative recombination is limited by the availability of carriers and not of the states. From a qualitative point of view, it is nothing but expected that the PL peak is somewhat shifted to lower energies compared with the bandgap deduced from the absorption measurements.

V. Solar Cells

Fig. 5 depicts the characteristics of some of the solar cells obtained with the fabrication methods presented in Section III. In Fig. 5(a), the current–voltage characteristics are shown, Fig. 5(b) shows the corresponding external QE measurements, Fig. 5(c) shows the temperature dependence of the open-circuit voltage, and Fig. 5(d) shows the temperature dependence of the short-circuit current density of sample C. The solar cell parameters of all solar cells presented in this paper can be found in Table I. Solar cells A and B have been fabricated with the process depicted in Fig. 1(b), whereas solar cell C has been fabricated with the process in Fig. 1(c). In all cases, a solar cell efficiency exceeding 6.5% has been achieved. However, there are some important differences between the devices. Solar cell A exhibits the highest open-circuit voltage and the lowest current density. The device fabricated with the process shown in Fig. 1(c) exhibits a high J_{SC} value; however, the voltage is slightly reduced. Solar cell B can be considered as a compromise between the devices A and C. The measured fill factors are comparable with the current record devices [7].

TABLE I
Solar Cell Parameters of the Devices That are Discussed Throughout the Paper

Device	η [%]	V_{OC} [mV]	J_{SC} mA/cm^2	FF [%]
A	6.7	365	29.6	62
B	6.7	348	32.5	59
C	7.1	324	35.8	61
D	2.7	238	24.8	46
E	4.6	303	30.3	50
F	6.2	318	34.1	57
G	6.0	283	36.3	58

First, we discuss the differences between the devices A and B fabricated with the same type of process. The current densities between the different devices can be traced back to different collection properties. This is clearly visible in Fig. 5(b), where the QE measurements are shown. The main differences are in the low-energy region of the QE, which is determined by absorption and collection. This finding is consistent with the doping densities deduced for the two devices. Sample A exhibits a very high doping density of approximately 3×10^{17} 1/cm^3, while in sample B, the doping density is reduced to roughly 5×10^{16} 1/cm^3. A high doping density in combination with a short carrier lifetime leads to significant losses in collection and, thus, in the current density and results in a poor low-energy response in the QE [23]. It is interesting to note that the device with the highest doping density exhibits the highest V_{OC}. Consequently, tunneling enhanced recombination is not high enough to deteriorate the voltage. The measured difference in doping is consistent with the findings by Brammertz *et al.* [24], who showed that that p-doping is increased with increasing Zn/Sn ratio. In our case, process A exhibits Zn/Sn ratio of roughly 1.17, whereas sample B exhibits a Zn/Sn ratio of 1.01. Sample C shows the best collection property and the highest current density. The composition is, according to the EDX analysis, slightly Sn-rich (Zn/Sn = 0.96). This is also in line with the findings by Brammertz *et al.* [24]. However, one has to keep in mind that the composition is measured with EDX. At 20-kV acceleration voltage, the penetration depth of the impinging electrons is equal to the film thickness (roughly 1 μm) as deduced with the program CASINO [25]. Therefore, the composition measured with EDX does not only include the CZTSe absorber but the ZnSe segregation at the back contact as well. The observed correlation with the Zn/Sn ratio refers to the global composition of the film, including the secondary phases at the back contact. We are, therefore, unable to uncover the controlling mechanism of the doping of CZTSe, since we cannot accurately measure the CZTSe composition.

The most intriguing finding is, however, the bandgap of the devices. A linear extrapolation of the low-energy slope of the QE yields a value of 0.86 $\pm$ 0.01 eV for all three samples. Some authors use the inflection point of the QE as a measure for the bandgap. In this case, a value of 0.94 $\pm$ 0.01 eV can be found. Both values are much lower than the current record device by Brammertz *et al.*, who measured a bandgap of roughly

1.0 eV [7]. As expected, the linear extrapolation of the QE yields smaller values than the inflection point determination. The value of the inflection point determination is consistent with the value of the bandgap from the absorption measurements, whereas the linear extrapolation is in line with the bandgap deduced from the PL measurements indicating that the band tails contain a significant amount of delocalized states.

The temperature dependence of the open-circuit voltage is depicted in Fig. 5(c). We observe a roll-over of the V_{OC} at roughly 130 °C. At higher temperatures, a linear increase of the V_{OC} with decreasing temperature is observed. The V_{OC} roll-over is accompanied with a strong drop of J_{SC} at low temperatures. This drop is due to an increase in series resistance as a consequence of carrier freeze out or a blocking barrier [26], [27].

An extrapolation of the V_{OC} to 0 K yields a value of 0.85 eV. This value is equal to the activation energy ϕ_B of the dominant generation/recombination pathway. If the value is equal to the bandgap E_G of the semiconductor, the device is not limited by dominant interface recombination. If the value is significantly lower than the bandgap, then there is either an unfavorable cliff like conduction band offset present at the CdS/CZTSe heterointerface or the device is limited by Fermi level pinning [23]. The deduced activation energy is equal to the RT-PL peak and is also equal to the linear extrapolation of the low-energy slope of the QE. As a consequence, it has been argued that the absorber is not limited by dominant interface recombination, since $\phi_B = E_G$ [28]. Here, we present a new insight, namely that the bandgap deduced from the absorption coefficient is higher than the bandgap measured from PL. This has also been reported for hydrazine-processed CZTSSe devices [4]. The lower peak position in PL is, according to [4], likely to be associated with the strong band tailing in the absorbers. Significant disorder in the Cu/Zn distribution may play a role. Comparing the deduced activation energy from V_{OC} versus T with bandgap deduced from absorption measurements suggests dominant interface recombination, whereas the linear extrapolation of the low-energy slope of the QE suggests dominant bulk recombination. In a semiconductor with strong tailing, it is not *a priori* clear which energy should be used to compare with the activation energy obtained from the V_{OC} extrapolation. Clearly, ϕ_B is smaller than the optical bandgap obtained from extrapolating the absorption in extended bandstates at higher energies. However, the energy of the radiative bulk recombination is measured by the PL. This energy agrees with the low-energy edge of the QE spectrum, which shows the states that contribute to the transport. Since the energy deduced from QE and the energy deduced from PL (with a k-value larger than 1) agree reasonably well, we can assume that the number of tail states is so large that they are, to a large degree, delocalized and contribute to transport. Consequently, the energy deduced from PL and QE is the energy that determines recombination in the bulk, i.e., the activation energy of the reverse saturation current. ϕ_B has to be compared with this bulk recombination energy. Since they agree, we can conclude that the device is limited by bulk recombination, although ϕ_B is smaller than the optical bandgap, describing the extrapolation of extended states. However, we note that further investigations related to concentration of the tail states, their degree of delocalization, and their spatial distribution within the absorber is certainly necessary. From our analysis, we cannot rule out that the tail states are still localized. Our conclusion is only based on the comparison of the QE, PL, and the V_{OC} versus T analysis.

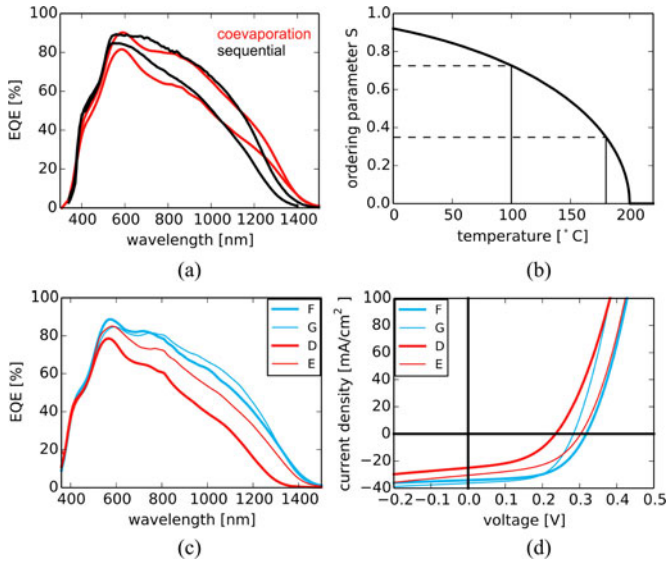

Fig. 6. (a) Comparison of coevaporated devices with devices produced by a sequential process. (b) Evolution of the ordering parameter as a function of the temperature according to the Vineyard model. (c) and (d) *I–V* curves corresponding QE measurements of devices with different types of low-temperature postannealings.

Finally, the effect of disorder in CZTSe will be analyzed a bit further. We have already seen that CZTSe exhibits a large amount of tail states with very large Urbach energies similar to amorphous material systems. The disorder is at least partly due to Cu atoms on Zn positions and *vice versa*. An order–disorder transition has been identified in CZTS and CZTSe. Here, we concentrate on selenium-based absorbers, where the transition temperature is at 200 °C [11]. First, we discuss the results from two different fabrication methods in our laboratory followed by some dedicated postdeposition annealing sequences in order to test how annealing affects the disorder and the solar cell parameters. Fig. 6(a) shows QE measurements of two devices prepared by the coevaporation routine presented in this paper and two devices from a sequential process. The sequential process has been described in detail in [3] and [29] and consists of coevaporation process at 320 °C, followed by a high-temperature annealing in a tube furnace at roughly 500 °C. It is clearly visible that 1) the two devices produced by the sequential process exhibit different apparent bandgaps and 2) that the high-temperature coevaporation devices exhibit even lower bandgaps. We believe that the difference between the different bandgaps can be traced back to different cooling rates after absorber growth or postannealing. As already discussed in Section II, the absorbers produced via high-temperature coevaporation can be considered as disordered, since after the process, the samples are cooled down to 200 °C, followed by quenching due to the removal of the substrate holder from the reactor chamber. The samples produced with the sequential process have an average cooling

rate from 200 °C to 50 °C of more than 1 h. However, until now, not much care had been devoted to the low-temperature cool down. Therefore, the given value can only be considered as a rough approximation. Nevertheless, the bandgaps of the devices are already significantly different between the coevaporated and the sequential devices. The sequential devices have a somewhat higher bandgap, which is consistent with the finding that an increased ordering, due to a slower cool down to RT, increases the bandgap of the absorbers.

In order to investigate how slow cool down affects the ordering and the photovoltaic properties of the devices, a few dedicated postdepostion annealings have been performed. In order to give a guidance of how the ordering changes upon annealing, we use the formalism introduced by Vineyard [30] to describe the order–disorder kinetics in a second-order phase transition. We assumed that the disorder in CZTSe is only in the pure Cu/Zn planes. If one assumes a square 2-D lattice, the order parameter S defines the ratio of Cu (Zn) atoms on Cu(Zn)sites. If all Cu and Zn sites have a 50% Cu and 50% Zn occupancy, the order parameter is zero, whereas if the all atoms are on the correct places, the order parameter is $S = 1$. The evolution of the order parameter for an order–disorder transition at 200 °C is depicted in Fig. 6(b). Upon cool down, the system slowly starts to order. The black curve depicts the thermodynamic limit for a specific temperature, i.e., the maximum ordering. In order to reach the thermodynamic limit, the sample has to be kept a long time at a specific temperature. More details on the kinetics of the annealing can be found in [11]. In this study, we have chosen the following annealing. Sample D has been produced with the process presented in Fig. 1(c) but has been cooled down from 200 °C to 100 °C over a period of 60 h in order to investigate the effect of a long and slow cool down. The EQE and the solar cell characteristics are shown in Fig. 6(c) and (d). We observe a shift in the QE by roughly 100 nm. However, the solar cell efficiency is much lower than the samples grown by the standard procedure with fast cool down and by removing the sample from the substrate heater. The solar cell efficiency is reduced by more than a factor of 2 compared with absorbers prepared in a similar matter (compare Table I). The annealing changes the ordering and the bandgap but does not improve the quality of the solar cell, V_{OC} and FF degrades, and the current is reduced due to the higher bandgap. The long cool down has been done without a significant Se partial pressure available. Therefore, one might conclude that the quality, i.e., the ordering, improves but the near surface region degrades due to some Se losses. Therefore, the same absorber has been reintroduced into the MBE chamber, and an additional 18 h of postanneal have been carried out at a substrate temperature of nominally 180 °C without additional selenium. This should, according to Fig. 6(b), reduce the ordering substantially. The resulting solar cell labeled E is depicted in Fig. 6(c) and (d). The QE shifted back to the low bandgap value. However, we do see a slightly higher bandgap than in the as-grown samples without any postannealing. However, as indicated in Fig. 6(b), we also expect that some ordering is still present in the absorbers. Interestingly, all solar cell parameters increased again and a 4.6% solar cell could be achieved. Therefore, the question remains as to how these solar cell parameters can be related to devices without postannealing. Therefore, another set of samples have been prepared via high-temperature coevaporation. Sample F has been removed right after the process without any additional postdeposition annealing. Afterward, one piece has been remounted into the vacuum chamber and postannealed at 180 °C for 18 h without additional Se (sample G). Again, we see a decrease in the solar cell efficiency after postdeposition annealing. The main losses of the device are in the open-circuit voltage, i.e., the recombination increases. The question is: Why we do not observe an improvement for the ordered samples? At this point of time, this question is difficult to answer. However, we need to test if a Se partial pressure during annealing is beneficial and a detailed band alignment study of the ordered and disordered samples have to be carried out. Since the bandgap shifts by more than 100 meV, the alignment of the CZTSe with the CdS buffer layer can change from a type I interface to a type II interface. This is an alternative explanation for the observed losses in V_{OC}. In any case, the disorder cannot be prevented since a solar cell module is operated at roughly 60 °C, which is far above the temperature where a high amount of ordering can be expected. Therefore, efforts have to be undertaken to improve the absorber and the heterojunction such that the efficiency of solar cell under working conditions is maximized.

VI. Conclusion

In this paper, a detailed high-temperature coevaporation study of $Cu_2ZnSnSe_4$ has been presented. Solar cell efficiencies exceeding 7% have been presented. In analogy to former investigations [6], the coevaporation growth sequence needs to be divided into at least two parts, i.e., a part where all elements are coevaporated and a part where only Sn, SnSe, and Se are coevaporated. We have shown that this can be accomplished in a two-step process, but also in a multiple step process with many iterations. Despite the lower onset temperature, we observe that Sn is not incorporated during the initial period of growth. The incorporation of Sn can be monitored with laser light scattering. Due to the failure of the Sn incorporation in the beginning of the process, we observe a lot of ZnSe at the Mo/CZTSe interface. We measure strong band tailing in the CZTSe absorbers in analogy to CZTSSe absorbers [4], and we deduce a bandgap if 0.93 eV from absorption measurements. This value does not coincide with room temperature PL peak position, which is 100 meV lower than measured from absorption. The temperature dependence of the open-circuit voltage reveals that the activation energy of the dominant recombination/generation process is equal to the room temperature PL value but smaller than the optical bandgap measured from absorption measurements. Due to the strong band tailing in CZTSe, no unambiguous conclusion of the dominant recombination path can be drawn. Currently, we assume that the dominant recombination path is not interface limited, since the activation energy of the generation/recombination path is equal to the transport bandgap deduced from QE. Finally, we observe smaller bandgaps than those reported in the literature due to the quenching of the absorber after fabrication, which leaves the absorber in a dominantly disordered state. We performed

low-temperature postannealings in order to change the ordering in the Cu/Zn planes. We can shift the bandgap measured from QE by roughly 100 meV to higher values. The change of the bandgap is reversible. Until now, we have found that the more ordered devices show an inferior performance compared with the less-ordered ones. However, we have to emphasize that extensive measurements have to be carried out before a full picture of the effect of disorder in CZTSe solar cells can be drawn.

ACKNOWLEDGMENT

M. Thevenin and T. Schuler are acknowledged for technical support and CdS and ZnO deposition. M. Kirsch at HZB Berlin is acknowledged for solar cell finishing of some of the devices. All authors are members of the Physics and Material Research Unit of the University of Luxembourg.

REFERENCES

[1] M. A. Green, K. Emery, Y. Hishikawa, W. Warta, and E. D. Dunlop, "Solar cell efficiency tables (version 43)," *Prog. Photovoltaic, Res. Appl.*, vol. 22, pp. 1–9, 2014.

[2] I. Repins, M. J. Romero, J. V. Li, S.-H. Wei, C.-S. J. D. Kuciauskas, C. Beall, C. DeHart, W.-C. H. J. Mann, G. Teeter, A. Goodrich, and R. Noufi, "Kesterite successes, ongoing work, and challenges: A perspective from vacuum deposition," *IEEE J. Photovoltaics*, vol. 3, no. 1, pp. 439–445, Jan. 2013.

[3] M. Mousel, T. Schwarz, R. Djemour, T. P. Weiss, J. Sendler, J. C. Malaquias, A. Redinger, O. Cojocaru-Mirédin, P. Choi, and S. Siebentritt, "Cu-rich precursors improve Kesterite solar cells," *Adv. Energy Mater.*, vol. 4, pp. 1300543-1–1300543-6, 2014.

[4] T. Gokmen, O. Gunawan, T. K. Todorov, and D. B. Mitzi, "Band tailing and efficiency limitation in kesterite solar cells," *Appl. Phys. Lett.*, vol. 103, pp. 103506-1–103506-5, 2013.

[5] S. Oueslati, G. Brammertz, and M. Buffière, *Thin Solid Films*, 2014, submitted for publication.

[6] I. Repins, C. Beall, N. Vora, C. D. Hart, D. Kuciauskas, P. Dippo, B. To, J. Mann, W.-C. Hsu, A. Goodrich, and R. Noufi, "Co-evaporated $Cu_2ZnSnSe_4$ films and devices," *Sol. Energy Mater. Sol. Cells*, vol. 101, pp. 154–159, 2012.

[7] G. Brammertz, M. Buffière, S. Oueslati, H. ElAnzeery, K. Ben Messaoud, S. Sahayaraj, C. Köble, M. Meuris, and J. Poortmans, "Characterization of defects in 9.7% efficient $Cu_2ZnSnSe_4$-CdS-ZnO solar cells," *Appl. Phys. Lett.*, vol. 103, no. 16, pp. 163904-1–163904-4, 2013.

[8] B. Shin, Y. Zhu, N. A. Bojarczuk, S. J. Chey, and S. Guha, "Control of an interfacial $MoSe_2$ layer in $Cu_2ZnSnSe_4$ thin film solar cells: 8.9% power conversion efficiency with a tin diffusion barrier," *Appl. Phys. Lett.*, vol. 101, pp. 053903-1–053903-4, 2012.

[9] R. Djemour, A. Redinger, M. Mousel, L. Gütay, and S. Siebentritt, "Multiple phases of $Cu_2ZnSnSe_4$ detected by room temperature photoluminescence," *J. Appl. Phys.*, vol. 116, pp. 073509-1–073509-9, 2014.

[10] J. J. S. Scragg, L. Choubrac, A. Lafond, T. Ericson, and C. Platzer-Björkman, "A low-temperature order-disorder transition in Cu_2ZnSnS_4 thin films," *Appl. Phys. Lett.*, vol. 104, pp. 041911-1–041911-4, 2014.

[11] G. Rey, A. Redinger, J. Sendler, T. P. Weiss, M. Thevenin, M. Guennou, B. E. Adib, and S. Siebentritt, "The band gap of $Cu_2ZnSnSe_4$: Effect of order-disorder," *Appl. Phys. Lett.*, vol. 105, pp. 112106-1–112106-4, 2014.

[12] A. Redinger, D. M. Berg, P. J. Dale, and S. Siebentritt, "The consequences of Kesterite equilibria for efficient solar cells," *J. Amer. Chem. Soc.*, vol. 133, pp. 3320–3323, 2011.

[13] W.-C. Hsu, I. Repins, C. Beall, C. DeHart, B. To, W. Yang, Y. Yang, and R. Noufi, "Growth mechanisms of co-evaporated kesterite: A comparison of Cu-rich and Zn-rich composition paths," *Prog. Photovoltaic, Res. Appl.*, vol. 22, pp. 35–43, 2012.

[14] J. I. Pankove, *Optical Processes in Semiconductors*. New York, NY, USA: Dover, 2012.

[15] A. Redinger, K. Hönes, X. Fontané, V. Izquierdo-Roca, E. Saucedo, N. Valle, A. Pérez-Rodríguez, and S. Siebentritt, "Detection of a ZnSe secondary phase in coevaporated $Cu_2ZnSnSe_4$ thin films," *Appl. Phys. Lett.*, vol. 98, pp. 101907-1–101907-3, 2011.

[16] G. Kaune, S. Hartnauer, and R. Scheer, "In situ XRD investigation of $Cu_2ZnSnSe_4$ thin film growth by thermal co-evaporation," *Phys. Status Solidi A*, vol. 211, pp. 1991–1996, 2014.

[17] G. Kaune, S. Hartnauer, F. Syrowatka, and R. Scheer, "Phase formation in $Cu_2ZnSnSe_4$ thin films deposited with multi-stage co-evaporation processes," *Sol. Energy Mater. Sol. Cells*, vol. 120, pp. 596–602, 2014.

[18] D. M. Bishop, B. E. McCandless, T. C. Mangan, K. Dobson, and R. Birkmire, "Effects of growth conditions on secondary phases in CZTSe thin films deposited by co-evaporation," *MRS Proc.*, vol. 1538, pp. 75–82, 2013.

[19] F. Urbach, "The long-wavelength edge of photographic sensitivity and of the electronic absorption of solids," *Phys. Rev.*, vol. 92, pp. 1324–1333, 1953.

[20] D. Adler, *Semiconductors and Semimetals c21*. New York, NY, USA: Academic, 1984.

[21] S. Schorr, "The crystal structure of kesterite type compounds: A neutron and X-ray diffraction study," *Sol. Energy Mater. Sol. Cells*, vol. 95, pp. 1482–1488, 2011.

[22] D. Abou-Ras, T. Kirchartz, and U. Rau, *Advanced Characterization Techniques for Thin Film Solar Cells*. New York, NY, USA: Wiley-VCH, 2011.

[23] R. Scheer and H. W. Schock, *Chalcogenide Photovoltaics*. New York, NY, USA: Wiley-VCH, 2011.

[24] G. Brammertz, Y. Ren, M. Buffière, S. Mertens, J. Hendrickx, H. Marko, A. E. Zaghi, N. Lenaers, C. Köble, M. M. J. Vleugels, and J. Poortmans, "Electrical characterization of $Cu_2ZnSnSe_4$ solar cells from selenization of sputtered metal layers," *Thin Solid Films*, vol. 535, pp. 348–352, 2013.

[25] D. Drouin, A. R. Couture, D. Joly, X. Tastet, V. Aimez, and R. Gauvin, "CASINO V2.42—A fast and easy-to-use modeling tool for scanning electron microscopy and microanalysis users," *Scanning*, vol. 29, pp. 92–101, 2007.

[26] T. P. Weiss, A. Redinger, J. Luckas, M. Mousel, and S. Siebentritt, "Admittance spectroscopy in kesterite solar cells: Defect signal or circuit response," *Appl. Phys. Lett.*, vol. 102, pp. 202105-1–202105-4, 2013.

[27] O. Gunawan, T. Gokmen, C. W. Warren, J. D. Cohen, T. K. Todorov, D. A. R. Barkhouse, S. Bag, J. Tang, B. Shin, and D. B. Mitzi, "Electronic properties of the $Cu_2ZnSn(Se,S)_4$ absorber layer in solar cells as revealed by admittance spectroscopy and related methods," *Appl. Phys. Lett.*, vol. 100, pp. 253905-1–253905-4, 2012.

[28] A. Redinger, M. Mousel, M. H. Wolter, N. Valle, and S. Siebentritt, "Influence of S/Se ratio on series resistance and on dominant recombination pathway in $Cu_2ZnSn(SSe)_4$ thin film solar cells," *Thin Solid Films*, vol. 535, pp. 291–295, 2013.

[29] A. Redinger, D. M. Berg, P. J. Dale, R. Djemour, L. Gütay, T. Eisenbarth, N. Valle, and S. Siebentritt, "Route towards high efficiency single phase $Cu_2ZnSn(S,Se)_4$ thin film solar cells: Model experiments and literature review," *IEEE J. Photovoltaics*, vol. 1, no. 2, pp. 200–206, Oct. 2011.

[30] G. H. Vineyard, "Theory of order-disorder kinetics," *Phys. Rev.*, vol. 102, pp. 981–992, 1956.

Authors' photographs and biographies not available at the time of publication.